IEEE Access
Multidisciplinary | Rapid Review | Open Access Journal

Received August 26, 2021, accepted September 7, 2021, date of publication September 17, 2021,
date of current version September 28, 2021.

Digital Object Identifier 10.1109/ACCESS.2021.3113646

Wi-Buoy: An Energy-Efficient Wireless Buoy Network for Real-Time High-Rate Marine Data Acquisition

VARUN AMAR REDDY[1] AND GORDON L. STÜBER[2], (Fellow, IEEE)
[1]Qualcomm Wireless Research Group, San Diego, CA 92121, USA
[2]School of Electrical and Computer Engineering, Georgia Institute of Technology, Atlanta, GA 30318, USA

Corresponding author: Varun Amar Reddy (varunama@qti.qualcomm.com)

This work was performed/supported by the authors at Georgia Institute of Technology, Atlanta, USA.

ABSTRACT The next frontier of maritime networking will see the deployment of large-scale buoy-based mesh networks, with an equal emphasis on both high-speed data transfer and energy-efficiency. One such challenging application is the operation of maritime seismic surveys for oil/gas exploration and academic studies. Large amounts of seismic data are generated at a rate of several Gigabits per second, by nearly 10,000–30,000 seismic sensors that are deployed on the seabed across an area of several hundred square kilometers in offshore oceanic environments. The task of monitoring existing reservoirs and identifying new oil and gas deposits require subsurface images of superior quality, which in turn are dependent on high-quality data for processing. Wireless technology can unlock real-time data transfer for rapid image-viewing, enhanced productivity, and reduced logistical costs. This interdisciplinary article outlines the challenges of marine seismic acquisition and the design of a buoy-based wireless backhaul network for high-rate data transfer over the ocean surface. Based on off-the-shelf IEEE 802.11 systems, a standards-compliant wireless buoy network architecture called *Wi-buoy* is proposed for real-time, scalable, and energy-efficient data delivery. In order to attain optimal power conservation, a *Buoy-Based Power-Saving Backhaul (B-PSB)* scheme is also proposed for specifying the operating parameters across all layers of the protocol stack. Essential aspects of the marine propagation environment are reviewed, and the performance of the proposed system is evaluated as a function of the antenna height, wind speed, compression ratio, and various flavors of the IEEE 802.11 standard. Furthermore, the use of Autonomous Underwater Vehicles (AUVs) is analyzed as an integral component of upcoming high-speed buoy-based networks in the maritime environment.

INDEX TERMS Wireless LAN, marine communication, power saving, access protocols, wireless backhaul.

I. INTRODUCTION

Radio-equipped buoys have long been used for navigation and environmental monitoring in offshore scenarios. Although low-rate data transfer between buoys can be achieved across large areas in a reliable manner, the true potential of high-speed wireless data delivery is yet to be realized in complex applications such as marine seismic acquisition.

Oil and gas are vital necessities for the sustenance of the global economy. With the proliferation of devices and machines that are dependent on these resources, seismic surveys have been witnessing an increase in the survey area along with the density of seismic sensor nodes such as *geophones* and *hydrophones* [1]. Given that 71% of the Earth's surface is covered by water bodies, maritime seismic surveys are frequently conducted by various geophysical services companies for identifying new oil and gas deposits. Apart from seismic exploration, maritime surveys also help monitor and characterize existing reservoirs. In recent years, *ocean bottom seismic (OBS)* acquisition has emerged as a superior source of high-quality data [2], where *ocean bottom cables (OBCs)* equipped with seismic sensors are laid directly on the seabed. Current implementations require the use of a dedicated recording vessel that is connected to the OBCs, albeit at a high cost and support for small-scale surveys alone. A more economical and scalable approach involves the use of anchored *source bouys (SBs)* that are attached to

The associate editor coordinating the review of this manuscript and approving it for publication was Zhenzhou Tang.

the OBCs [1]. Uncompressed seismic data is then manually transferred from each of the buoys at the end of the survey, at the sacrifice of real-time data processing capability.

The application of wireless buoy networks in OBS acquisition has received little attention, where a few works [3], [4] have provided solutions for the delivery of small amounts of quality-control (QC) information and not the entirety of the seismic dataset in real-time. This arises from the fact that unlike typical low-rate sensor networks, data is generated at a rate of several Gigabits per second across an area of $150 - 300$ km^2 [5], [6]! Moreover, a description of the specific protocol and any power-saving mechanism has not been provided in [3], [4]. Although several wireless systems have already been proposed for onshore land-based seismic acquisition [6]–[8], there continues to be a dearth of wireless technology that can achieve real-time high-quality seismic data delivery in marine OBS acquisition systems.

Several additional approaches, outside the domain of marine seismic acquisition, are of considerable interest as well. A review of maritime networking is provided in [9], [10] from the perspective of the upper layers of the protocol stack. Experimental results are provided in [11], [12], where the former work considers a coastal scenario, while the latter work has taken into account the impact of wind speeds on long-range communication. An energy-efficient system based on satellites, UAVs, and terrestrial base stations was studied in [13], that is geared towards 6G coverage for maritime communications near the coastline. Along similar lines, although 4G or 5G networks are attractive options, their licensed nature limit their use in seismic surveys, as opposed to unlicensed technologies such as IEEE 802.11 or Ultra-Wideband [3], [6]–[8]. Low power wide area networks offer a promising solution in terms of the power consumption and range, but cannot support high-rate data transfer.

While current literature has extensively analyzed the feasibility of long-range marine communication, along with energy-harvesting capabilities, sufficient emphasis has not been laid on conserving power in such buoy-based mesh networks. Furthermore, there is a dearth of analysis on the interplay between achieving high data rates, effective power-saving, and low latency in large-scale maritime surveys.

With the above motivation in mind, this article provides an overview of a challenging yet relevant application of marine seismic acquisition, and the related nature of the maritime propagation channel. A primary contribution of this article is a wireless buoy network architecture called *Wi-Buoy* that can achieve real-time, high-rate, and energy-efficient marine data acquisition, via Radio Frequency (RF) communication links over the ocean surface. The use of recently proposed technologies such as Autonomous Underwater Vehicles (AUVs) [14] are also evaluated and incorporated into *Wi-Buoy*. The proposed architecture is compliant with the IEEE 802.11 standard and can be augmented by the *Buoy-Based Power Saving Backhaul (B-PSB)* scheme to attain optimal power conservation performance through a cross-layer design. The IEEE 802.11 protocol suite is an ideal choice given its unlicensed nature, low cost, high data rate capability, and widespread availability of off-the-shelf hardware. Furthermore, a standards-compliant solution promotes simpler and economical deployment.

Various resource allocation problems are formulated and solved to minimize the total power consumption under a latency constraint, including modifications to the backhaul scheme proposed in our previous work for onshore seismic surveys [15]. These enhancements in the B-PSB scheme include incorporating the routing aspect at the network layer, co-channel interference (CCI) mitigation approaches, the use of external nodes such as AUVs, and the impact of the marine propagation environment. The efficacy of *Wi-Buoy* is illustrated through a performance evaluation over multiple unlicensed frequency bands using protocols such as IEEE 802.11af, 802.11n, 802.11ax, and 802.11ad. The overall power conservation performance is also evaluated in terms of the antenna height and Sea State Codes (SSCs), as prescribed by the World Meteorological Organization (WMO) [16]. The concepts described in this article can be applied to various other maritime applications and create new research opportunities.

The remainder of this paper is organized as follows. The topic of marine seismic acquisition and the related system requirements are reviewed in Section II. The proposed *Wi-Buoy* architecture is described in Section III, which comprises a detailed analytical model on the basis of which the B-PSB scheme is developed. The operation of AUVs and their compatibility with *Wi-Buoy* is also discussed. Lastly, a comprehensive performance evaluation is conducted in Section IV, following which the findings are summarized in the conclusion in Section V.

II. MARINE SEISMIC ACQUISITION

As shown in Fig. 1, a seismic vessel (SV) is a large ship that tows an array of *air guns* across the survey area. Air guns are mechanical devices capable of generating seismic signals, termed as a *sweep*. The seismic signals are reflected by subsurface layers and subsequently recorded by seismic sensors. The entire set of recorded data is aggregated at the SV and processed to generate an image of the subsurface. Conventional systems employ the use of *streamers* wherein a string of hydrophones are towed by the SV alongside the air guns. However, the azimuth angle is very limited and hydrophones can only capture the acoustic wavefield component. Furthermore, ghost reflections [1] are encountered at the ocean surface, which mandates the need for additional processing to eliminate the resultant interference.

These drawbacks can be overcome via the use of OBS acquisition [2], wherein OBCs are deployed directly on the seabed and 4-component (4C) sensors (comprising a 3C geophone and a hydrophone) are used to record both the acoustic and elastic wavefield components for obtaining high-quality images of the subsurface. The use of OBCs also enables 4D acquisition wherein the same survey area is repeatedly mapped over a period of time, thereby enabling

FIGURE 1. A seismic vessel (SV) is a specialized ship equipped with various types of equipment required for the acquisition process, and is typically 100 m in length with a crew size of 30-50 members [1].

preemptive acquisition by predicting the movement of subterranean deposits.

To ensure high-quality depth imaging, nearly 10,000–30,000 sensors are expected to be deployed over areas as large as 150-300 km^2 in OBS acquisition [5]. A sweep typically lasts for a duration of 8-12 s, called the *sweep length*. At the end of the sweep, the sensors record data for a duration of 4-6 s, known as the *listen time*. Meanwhile, the SV 'moves-up' to the next point where a sweep will be conducted, for a duration of 8-10 s, called the *move-up time*. As shown in Fig. 2, the sweep, listen, and move-up operations are repeated sequentially across the survey area. Given seismic acquisition requirements, an orthogonal deployment is considered where 4C sensors are positioned linearly along an OBC to form a *Receiver Line* (RL) [6], as shown in Fig. 3. The SV moves along *Source Lines* (SLs), which are perpendicular to the RLs.

AUVs are touted to become an important component of marine OBS acquisition systems in the future. A group of AUVs, each towing a string of hydrophones, can be operated at a certain depth to record low-noise data as compared to conventional streamers [14]. Although AUVs cannot capture the elastic wavefield component, they can complement OBS acquisition systems by enabling flexible receiver topologies. AUVs can also approach the seabed and collect data from standalone ocean bottom nodes (OBNs) [1] and gather QC data pertaining to any oil pipes or other related infrastructure.

A. WIRELESS NETWORK REQUIREMENTS FOR MARINE SEISMIC ACQUISITION

The following system requirements are influenced by both aspects of wireless networking and marine seismic acquisition.

- *Real-Time Data Delivery:* A desirable feature would be to receive all the recorded seismic data at the SV in real-time (by the end of the subsequent sweep cycle). With a sophisticated on-board processing system, the crew can get a first-hand look at the seismic images without having to wait for prolonged periods to analyze the seismic traces. Real-time acquisition at the SV can enable scenarios where a group of AUVs is guided to a desired location and depth [14] to re-sweep a specific region and generate seismic images of enhanced quality. Additionally, real-time QC data can help detect faulty equipment and inspect the battery life of the sensors, the recording parameters, and most importantly the seismic background noise [1]. Proactively applying seismic noise-suppression techniques can eliminate the need for re-sweeping which in turn provides a phenomenal improvement in the surveying efficiency.
- *High-Throughput:* Given a sampling frequency of 2 kHz and a 24-bit analog-to-digital converter, a 4C sensor would generate data at a rate of 192 Kbps. Although the data rate per sensor may seem insignificant, the aggregate data rate at the SV lies in the range of $0.3 - 2$ Gbps. Hence, the wireless system must be able to sustain Gigabit-rate data transfer in order to achieve real-time data delivery.
- *Low Power Consumption:* Energy-efficient schemes are vital to extending the operational life of the buoys, as the duration of maritime surveys may stretch over several weeks.
- *Scalability:* By establishing coverage across large survey areas with minimal number of buoys, a scalable solution can reduce the overall cost and complexity of the system.
- *Open Standard:* Utilizing commercial off-the-shelf hardware over unlicensed bands can facilitate reduced costs, market penetration, and ease of deployment.
- *Support for New Technologies:* The proposed wireless network architecture must support diverse seismic technologies such as AUVs [14] and continue to achieve real-time data delivery.
- *Data compression:* Seismic data compression is a key enabling technology in large-scale surveys [17]. Lossy and lossless compression have both been analyzed in seismic acquisition with compression ratios of up to 60.
- *Natural conditions:* Maritime surveys are conducted during favourable weather conditions such as low wind speeds and wave heights. Rough weather not only affects the quality of the seismic data but also hampers the movement of the SV. Furthermore, the survey is halted when the presence of any animals (that depend on acoustic communication) is detected within the survey area [1], [5].

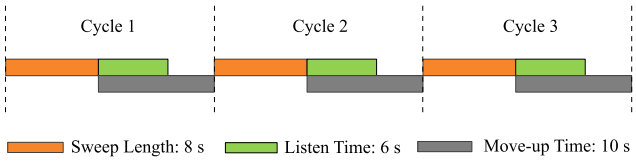

FIGURE 2. An illustration of single-fleet operation where the SV sequentially sweeps across the survey area [6].

III. WI-BUOY: AN ENERGY-AWARE SOLUTION FOR MARINE ACQUISITION VIA WIRELESS BUOYS

Firstly, the unique propagation environment, that occurs in maritime seismic surveys, is reviewed in subsection III-A. The topology and specifics of the proposed *Wi-Buoy* architecture are then described in subsection III-B, following which two distinct components of the architecture are analyzed in the remainder of the section.

A. PROPAGATION OVER THE SEA SURFACE

Various experimental characterizations of the wireless channel in multiple frequency bands for maritime communications have shown that large-scale fading effects are captured well by the two-ray propagation model, and small-scale fading due to diffuse multipath components such as wave motion can be characterized by the Rician distribution $R(s, \sigma)$ [18]–[23]. For a noise-limited system, the outage probability due to Rician fading is given by [24]

$$p_{out}^{Ri} = 1 - Q_M\left(\frac{s}{\sigma}, \frac{P_r - \mathrm{Rx}_{\min}}{\sigma}\right) \tag{1}$$

where $Q_M(\bullet, \bullet)$ denotes the Marcum Q-function, P_r denotes the received power, and $\mathrm{Rx}_{\min}$ denotes the minimum receiver sensitivity.

A Line-of-Sight (LoS) link between adjacent buoys may be obstructed by tall waves due to wind effects, particularly when low antenna heights are employed for logistical purposes. Analytical expressions for the probability of LoS were derived in [25] on the basis of the antenna height and wave action. It is seen that an antenna height of at least 1 m is required to yield LoS links under moderate conditions entailing wind speeds of up to 20 kmph. Given that the probability of a NLoS link due to wave blockage is denoted by p_{out}^{W}, the overall outage probability can be expressed as

$$p_{out} = 1 - \left(1 - p_{out}^{Ri}\right)\left(1 - p_{out}^{W}\right) \tag{2}$$

A unique phenomenon that is particularly common near the equator is the occurrence of evaporation and surface ducts [26]. These ducts provide the advantageous feature of trapping the radiation energy and extending the transmission range beyond the horizon over several tens of kilometers. However, it was shown in [26] that such a range extension is only achievable in the case of small grazing angles, failing which most of the radiated energy is refracted into the atmosphere. With a trapping beamwidth of less than 1°, the received power would be highly attenuated, particularly when the weather conditions (such as temperature and humidity) are erratic and the duct height fluctuates across the survey area. Overall, establishing reliable beyond-the-horizon communication through atmospheric ducts is highly contingent upon tight beamforming and prolonged duct stability, both of which may be inconceivable in large-scale maritime seismic surveys.

B. A MESH NETWORK OF WIRELESS BUOYS

In addition to the above shortcomings of duct-based communication, the duration of a seismic survey can range from a few days to several weeks, and the network architecture cannot always rely on the presence of a duct to facilitate long-range data transfer directly between the SBs and the SV. Hence, *Wi-Buoy* presents a flat mesh architecture of additional *relay buoys (RBs)*, as shown in Fig. 3, for providing coverage across the survey area. Each RB can be equipped with up to three radios to facilitate simultaneous reception and transmission over unique channels.

Referring to Fig. 3, the topology with respect to the SBs and SV is determined a-priori as per geophysical requirements [1]. In this study, a very large-scale survey is considered across an area of 30 × 10 square kilometers. The SBs are positioned every 200 m on one end of the survey over a length of 10 km. Each SB controls an OBC comprising a total of 600 sensors that are positioned in intervals of 50 m along the RL over a length of 30 km, resulting in a total of 30,000 sensors. The only mobile node in the network is the SV that sweeps across the survey area at a speed of 4.5–5 knots ($\approx$ 10 kmph). It is important to note that once the OBCs are deployed on the seabed, the SBs are effectively anchored and fixed to the OBCs for the duration of the survey. Meanwhile, the anchoring of the RBs is more flexible in the sense that they may be deployed at any position across the survey area.

While translational motion of the buoys is effectively constrained by anchoring, the same cannot be easily achieved for rotational motion. Hence, it would be preferable to utilize omnidirectional antennas, as opposed to a mechanically-controlled directional approach suggested in [3]. Alternatively, the use of phased arrays with electronically steerable beams is a far more attractive option for establishing directional links, provided that the form factor of the array is sufficiently small. The RBs can be arranged in a hexagonal tessellating pattern for compact coverage and to reduce the total number of devices. However, even a hexagonal topology cannot nullify the impact of CCI in a mesh network, where a worst-case signal-to-interference-plus-noise ratio (SINR) of −7 dB is observed under the effect of a two-ray propagation model with 4-cell reuse. One way to eliminate the impact of CCI is to exploit the curvature of the Earth and ensure that the co-channel cells are located beyond the horizon. Given an antenna height of h, the geometrical distance to the horizon is given by $\sqrt{2R_e h}$, where $R_e \approx 6370$ km is the mean radius of the Earth. Hence, the cell radius R, considering 4-cell reuse, would have to lie in the following range.

$$\sqrt{\frac{R_e h}{6}} < R \leq \sqrt{\frac{2R_e h}{3}} \tag{3}$$

C. ACQUISITION FROM THE SOURCE BUOYS

As shown in Fig. 3, a number of SBs that are within the communication range of the nearest RB can be grouped together

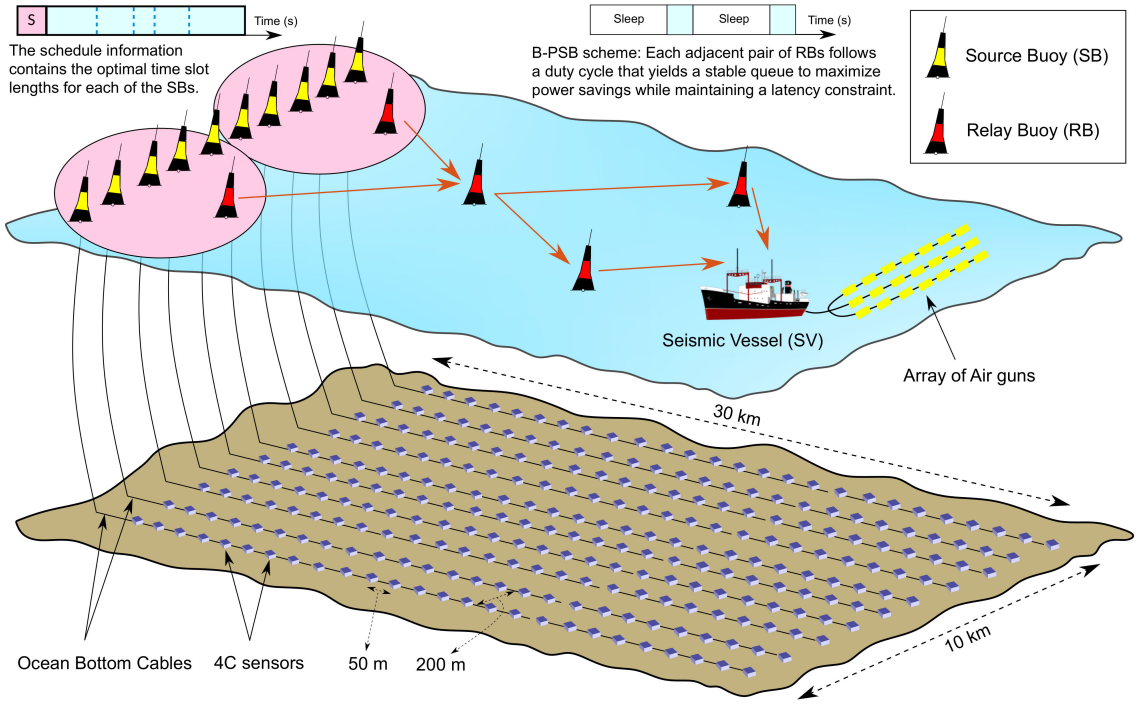

FIGURE 3. Proposed *Wi-Buoy* architecture: OBCs are attached to SBs floating on the surface, that transfer their data to the nearest RB using a TDMA-based approach. The data is then subsequently relayed by the RBs to the SV using the B-PSB scheme. Occasionally, AUVs may resurface and transfer their data in conjunction with the B-PSB scheme.

to transfer data over a common channel. The default channel access scheme provided by the IEEE 802.11 standard is the *Enhanced Distribution Channel Access (EDCA)* scheme [27], based on carrier sense multiple access with collision avoidance (CSMA/CA) along with a binary exponential backoff. In the presence of a large number of SBs, the contention process is exacerbated which in turn leads to an increased number of retransmissions and inefficient use of time and power resources.

To remedy this problem, a time division multiple access (TDMA) approach is proposed for deterministic channel access, that can nullify the effect of collisions and promote enhanced power conservation. For instance, a schedule can be broadcasted by the RB, comprising information about the time slot durations allocated to each of the SBs, using which an SB may transfer data during its allocated time slot and enter sleep mode for the remaining frame duration. A guard duration can also be included between adjacent time slots to account for any radio wake-up, hardware delays, and synchronization offsets. An optimization framework is developed in the following subsections to compute the time slot values, such that the total power consumption of the SBs is minimized.

In this paper, we consider a TDMA approach that can be implemented over the EDCA scheme in a standards-compliant manner by enforcing functionality at the application layer [28]–[30]. The same concept can be applied to channel reservation for inter-RB communication as well. Alternatively, some recent works regarding mesh networking in 802.11 are of interest [27], [31], [32]. As per the *Mesh Coordination Function Controlled Channel Access (MCCA)* scheme [27], periodic channel reservations can be made at the MAC layer, via the transmission of *Delivery Traffic Indication Map (DTIM)* beacons. These reservations are of a common duration and offset with respect to the start of the periodic time interval. Analytical models were developed in [31], [32] for the choice of the reservation parameters as a function of the required quality-of-service.

For the seismic data acquisition system under consideration, the deterministic nature of traffic being generated by the geophones, implies that the channel reservation scheme can be deterministic as well. Hence, by imposing a TDMA-based reservation scheme from the application layer, the need for periodic DTIM beacon transmissions between the buoys can be eliminated, along with the associated time and energy costs. Furthermore, the MCCA-based model is susceptible to interference from hidden nodes and lacks the flexibility of having unique time offsets for the reserved durations in a given interval, thereby preventing design opportunities for CCI mitigation (such as in Section III-D3). Lastly, an upper-layer-based reservation scheme can be implemented using widely available commercial off-the shelf hardware (typically employing the EDCA scheme) in a simpler and more economical manner.

1) AN ANALYTICAL MODEL FOR THE ACQUISITION TIME AND POWER CONSUMPTION

Before delving into the details of the optimization problem, analytical formulations for the acquisition time and power consumption are derived. In particular, the use

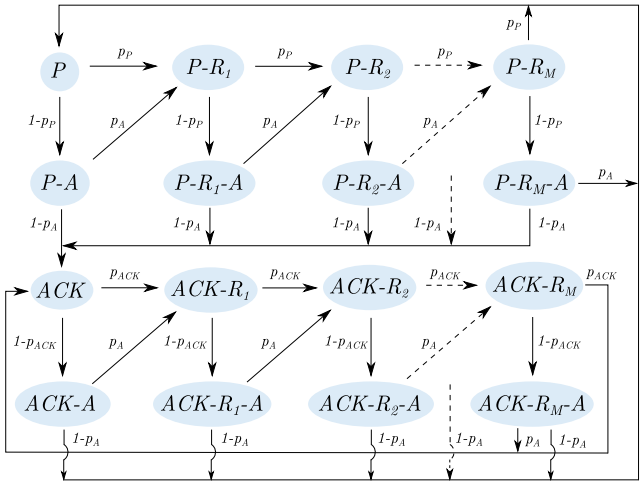

FIGURE 4. A Semi-Markov process representing TCP data transfer over the IEEE 802.11 EDCA with frame aggregation [15].

of Transmission Control Protocol (TCP) over the IEEE 802.11 Physical (PHY) and Medium Access Control (MAC) layers with frame aggregation is considered.

Frame aggregation is a technique utilized by the IEEE 802.11 standard to aggregate several payload segments into a single frame and boost the overall data rate by eliminating the recurrence of overhead [27]. At the MAC layer, data blocks are encapsulated to form MAC Service Data Units (MSDUs) that are aggregated to form an Aggregate MSDU (A-MSDU). Multiple such A-MSDUs can in turn be aggregated to form an Aggregate MPDU (A-MPDU) which is passed to the PHY layer for transmission. The number of MSDUs that are aggregated into the final payload can be defined as the *aggregation length*. Following the A-MPDU frame, a Block Acknowledgement Request (BAR) is sent by the transmitter, in response to which a Block Acknowledgement (BA) is sent back by the receiver. The BA contains a bitmap corresponding to those MPDUs that have failed reception, and would require retransmission.

For each transmission under EDCA, a backoff counter is drawn uniformly from the interval $[0, CW-1]$, where CW denotes the contention window size, and $CW \in [CW_{\min}, CW_{\max}]$. Initially, the value of CW is set to $CW_{\min}$, following which it is doubled up to a maximum of M retransmissions (when it attains the value of $CW_{\max}$). After a successful transmission is made, the value of CW is reset to $CW_{\min}$.

As shown in Fig. 4, a semi-Markov process [33] is used to represent the transmission of a TCP payload segment (denoted by P) and up to M 802.11 retransmissions (denoted by $P-R_m$, $1 \le m \le M$) along with the subsequent 802.11 acknowledgements (denoted by $P-A$ and $P-R_m-A$). This is followed by the TCP acknowledgement (denoted by ACK) and its associated 802.11 retransmissions and acknowledgements. The packet error probability p_S is a function of the packet size corresponding to state S and the SINR. In this analysis, the TCP congestion window is configured to match the value of the aggregation length, implying that packet collisions would not occur (since the TCP payload segment and acknowledgement would be sequentially transmitted back and forth). Hence, by assuming that there are no TCP timeouts and delayed TCP acknowledgements, the nature of p_S is determined by the perceived SINR alone since there are no collisions that are introduced as part of the contention process between any two communicating buoys.

Considering the states pertaining to the TCP payload segment, an expression for p_P can be formulated as the probability of all the A-MSDUs (within the A-MPDU) and the BAR being transmitted successfully.

$$p_P = 1 - \left\{ (1-\text{BER})^{\mathcal{S}_{\text{BAR}}} \times \prod_{i=1}^{\mathcal{N}_{\text{A-MS}}} (1-\text{BER})^{\mathcal{S}_{i,\text{A-MS}}} \right\} \tag{6}$$

$$p_A = 1 - (1-\text{BER})^{\mathcal{S}_{\text{BA}}} \tag{7}$$

where the various notations are listed in Table 1. An expression for p_{ACK} can be derived along similar lines.

For the l^{th} link, define the notation $\boldsymbol{\phi}_l \triangleq [K_l, \eta_l]$, where K_l and η_l denote the aggregation length and the Modulation and Coding Scheme (MCS) index respectively. The corresponding transmit power is denoted by Υ_l. Following the analysis in [15], and incorporating the impact of the marine propagation environment, an expression is derived for $t_{l,d}(\boldsymbol{\phi}_l)$, the time required by the l^{th} link for a single successful exchange of a TCP payload segment and its associated acknowledgement. Additionally, retransmissions at both the MAC and transport layers are accounted for.

$$t_{l,d}(\boldsymbol{\phi}_l) = t^{P}_{l,d}(\boldsymbol{\phi}_l) + t^{ACK}_{l,d}(\boldsymbol{\phi}_l) \tag{8}$$

$$t^{P}_{l,d}(\boldsymbol{\phi}_l) = \left(\frac{1}{1-p_{out}}\right) \times \left(\frac{1}{1-p_{P,\text{A-MS}}}\right) \times \left(\frac{\pi_P}{T_P(\boldsymbol{\phi}_l)} - \frac{\pi_{P-R_M}}{T_{P-R_M}(\boldsymbol{\phi}_l)} - \frac{\pi_{P-R_M-A}}{T_{P-R_M-A}(\boldsymbol{\phi}_l)}\right)^{-1} \tag{9}$$

$$P_{tx} = \frac{t^{P}_{l,d}}{t_{l,d}} \left(\sum_{s' \in S_P} \frac{\pi_{s'} E_{s',tx}}{T_{s'}} + \sum_{s' \in S_{P-A}} \frac{\pi_{s'} E_{s',rx}}{T_{s'}} \right) + \frac{t^{ACK}_{l,d}}{t_{l,d}} \left(\sum_{s' \in S_{ACK}} \frac{\pi_{s'} E_{s',rx}}{T_{s'}} + \sum_{s' \in S_{ACK-A}} \frac{\pi_{s'} E_{s',tx}}{T_{s'}} \right) \tag{4}$$

$$P_{rx} = \frac{t^{P}_{l,d}}{t_{l,d}} \left(\sum_{s' \in S_P} \frac{\pi_{s'} E_{s',rx}}{T_{s'}} + \sum_{s' \in S_{P-A}} \frac{\pi_{s'} E_{s',tx}}{T_{s'}} \right) + \frac{t^{ACK}_{l,d}}{t_{l,d}} \left(\sum_{s' \in S_{ACK}} \frac{\pi_{s'} E_{s',tx}}{T_{s'}} + \sum_{s' \in S_{ACK-A}} \frac{\pi_{s'} E_{s',rx}}{T_{s'}} \right) \tag{5}$$

TABLE 1. List of notations.

Notation	Description
$\mathcal{N}_{\text{A-MS}}$	Number of A-MSDUs in an A-MPDU
$\mathcal{S}_{i,\text{A-MS}}$	Number of bits in the i^{th} A-MSDU
$\mathcal{S}_{\text{BAR}}$	Number of bits in a BAR frame
$\mathcal{S}_{\text{BA}}$	Number of bits in a BA frame
T_S	Time duration of state S
$E_{S,tx}$	Energy consumption of state S in transmit mode
$E_{S,rx}$	Energy consumption of state S in receive mode
BER	Bit error rate

$$t_{l,d}^{ACK}(\boldsymbol{\phi}_l) = \left(\frac{1}{1-p_{out}}\right) \times \left(\frac{1}{1-p_{ACK,\text{A-MS}}}\right) \times \left(\frac{\pi_{ACK}}{T_{ACK}(\boldsymbol{\phi}_l)} - \frac{\pi_{ACK-R_M}}{T_{ACK-R_M}(\boldsymbol{\phi}_l)} - \frac{\pi_{ACK-R_M-A}}{T_{ACK-R_M-A}(\boldsymbol{\phi}_l)}\right)^{-1} \tag{10}$$

where π_S represents the proportion of time that the semi-Markov process spends in state S. The value of π_S is given by the weighted average of the steady-state probabilities, with the weights being the duration spent in each state [33]. The factor $1/(1-p_{out})$ accounts for the mean number of packets that are successfully transmitted under the impact of Rician fading and wave action. Similarly, the terms comprising the packet error probabilities, $p_{P,\text{A-MS}}$ and $p_{ACK,\text{A-MS}}$, account for the mean number of A-MSDUs that are successfully received within an A-MPDU. Lastly, expressions for the power consumption in transmit (P_{tx}) and receive (P_{rx}) modes are given in (4) and (5), as shown at the bottom of the previous page, respectively.

2) AN OPTIMIZATION FRAMEWORK FOR POWER CONSERVATION AT THE SBs

With the above formulations in place, the following optimization framework is derived to minimize the total power consumption for a given cell of radius R, comprising an RB and a total of L SBs. As per the value of R, the l^{th} SB can be assigned a maximum MCS index η_l such that the value of p_{out}^{Ri} in (1) does not exceed a given threshold $p_{out,th}$. In order to boost the performance of all SBs that are encumbered by a shared channel for data delivery to a single common RB, the transmit power and aggregation length are set to the maximum allowable values (denoted by Υ_{max} and K_{max} respectively). Hence, a linear optimization problem is expressed as follows.

$$\underset{[\tau_1,\,\tau_2,\,\cdots,\,\tau_L]}{\text{minimize}} \quad \sum_{l=1}^{L} P_{tx}(\eta_l)\cdot\tau_l + P_{sl}\cdot\left(\mathcal{C} - \tau_{gd} - \sum_{\substack{m=1\\m\neq l}}^{L}\tau_l\right) \tag{11}$$

$$\frac{\tau_l}{\Gamma(\eta_l)} \geq d_{\min} \geq Q \tag{12}$$

$$\mathcal{C} = \sum_{l=1}^{L}(\tau_l + \tau_{gd}) \tag{13}$$

where τ_l is the time slot duration allocated to the l^{th} SB, τ_{gd} is the guard interval between adjacent slots, and P_{sl} denotes the power consumed during sleep mode. Constraint (12) ensures that a minimum number of data packets (including quality control information Q) is transmitted by all the SBs. For a given MCS index, the data transmission time grows linearly with the aggregation length [15] i.e., $t_{l,d}(\boldsymbol{\phi}_l) = \Gamma(\eta_l)\cdot K_l$. Hence, the ratio $\tau_l/\Gamma(\eta_l)$ represents the mean number of successfully delivered data packets that is mandated to be at least $d_{\min}$. Lastly, constraint (13) ensures that the sum of all the time slot durations, along with their associated guard intervals, is equal to the total cycle length $\mathcal{C}$.

D. BUOY-BASED POWER-SAVING BACKHAUL (B-PSB) SCHEME

The preceding subsection dealt with a power-optimal approach for acquiring data from multiple SBs at the nearest RB. The collected data would have to be relayed through a mesh network of RBs towards the SV in an energy-efficient manner as well. The proposed B-PSB scheme accounts for the various challenges introduced by all layers of the protocol stack, and yields optimal operating values for the total number of required RBs, the transmit power and MCS index at the PHY layer, the aggregation length at the MAC layer, routing paths at the network layer, and the TCP congestion window size at the transport layer.

At its very core, the proposed B-PSB scheme employs a duty-cycling mechanism at each of the inter-RB links, as shown in Fig. 3. Each radio interface alternates between a short duration of bursty data transfer (either in transmit or receive mode) and a prolonged duration of sleep (where the transceiver is switched off) to conserve power while buffering incoming packets. Hence, the power consumed by the l^{th} link can be expressed as

$$P_l = \frac{2\gamma_{sl}(t_{l,sl} - t_{sl}^{min}) + 2\gamma_{idle}t_{sl}^{min} + \gamma_d(\boldsymbol{\theta}_l)t_{l,d}(\boldsymbol{\phi}_l)}{t_{l,sl} + t_{l,d}(\boldsymbol{\phi}_l)} \tag{14}$$

where t_{sl} denotes the sleep duration, which is lower-bounded by t_{sl}^{min} to account for the wake-up duration imposed by IEEE 802.11 chipsets [34]. The terms γ_{sl}, γ_{idle}, and $\gamma_d(\boldsymbol{\theta}_l)$ denote the power consumed in the sleep, idle, and active modes respectively, where the definition $\boldsymbol{\theta}_l \triangleq [\Upsilon_l, \eta_l, K_l]$ is introduced for ease of notation. The value of γ_d is simply given by the sum of P_{tx} and P_{rx} in (4)-(5).

1) LATENCY ANALYSIS

Concepts from queuing theory are employed in analysing the impact of t_{sl} on the latency and power consumption associated with each of the inter-RB links. Let the arrival and service rate of packets over the l^{th} link be denoted by λ_l and μ_l respectively. Since an A-MPDU is transmitted only once K_l packets have been buffered, the minimum *batch size* is given by K_l. Furthermore, the aggregated packets are transmitted in batches of size K_l as well. Hence, the transmission queue

at a node can be represented by a D/D$^{[K_l]}$/1 *batch service* model[1] [33].

To maintain queue stability, the service rate at a node must exceed the arrival rate of packets.

$$\mu_l = \frac{K_l}{t_{l,sl} + t_{l,d}(\boldsymbol{\phi}_l)} > \lambda_l \tag{15}$$

For any given $\boldsymbol{\theta}_l$, the value of P_l as given by (14) monotonically decreases with an increase in $t_{l,sl}$, since $\partial P_l / \partial t_{l,sl} < 0, \ \forall \ t_{l,sl} > 0$. Hence, minimum power consumption is achieved when the value of $t_{l,sl}$ is set to the largest value possible while maintaining queue stability.

$$t_{l,sl}(\boldsymbol{\phi}_l) = \frac{K_l}{\lambda_l} - t_{l,d}(\boldsymbol{\phi}_l) - \delta \tag{16}$$

where an arbitrarily small constant, δ, is introduced to satisfy (15). In the case of IEEE 802.11 systems, the value of δ can be set to the *slot time* which is the smallest standard-prescribed granularity in time.

The overall latency at the SV is given by the sum of the contributions of each of the constituent links that make up a given path. Considering a D/D$^{[K_l]}$/1 queue with $\mu_l > \lambda_l$, there is no queuing delay. Hence, the latency is solely given by the end-to-end transmission delay. For a given path denoted by $\mathcal{P}$, the maximum latency $\mathcal{L}_\mathcal{P}$ at the SV can be expressed as

$$\mathcal{L}_\mathcal{P} = \sum_{l \in \mathcal{P}} \left(\frac{K_l}{\lambda_l} - \delta \right) \tag{17}$$

2) ROUTING ACROSS THE RBs

An additional aspect that was not studied in [15] is the choice of the routing paths, since static routing is well-suited for an onshore seismic survey, where the use of vibroseis trucks leads to the frequent occurrence of obstructions. In the case of a maritime survey, the problem of determining the routing paths across the mesh of RBs should be integrated into the problem formulation as well. The expression for P_l can be rewritten by substituting the value of $t_{l,sl}$ from (16) into (14).

$$P_l = 2\gamma_{sl} + \frac{2(\gamma_{idle} - \gamma_{sl}) t_{sl}^{min} \lambda_l}{K_l - \lambda_l \delta} + \frac{(\gamma_d(\boldsymbol{\theta}_l) - 2\gamma_{sl}) t_{l,d}(\boldsymbol{\phi}_l) \lambda_l}{K_l - \lambda_l \delta} \tag{18}$$

As derived in Appendix V, it can be shown that the power consumption of a link monotonically increases with λ_l. Hence, the routing aspect can be incorporated in the form of a modified load-balancing problem, wherein some of the RBs may be altogether removed. The deterministic traversal pattern of the SV can also be exploited to compute the optimal routes a-priori and store them across the network as an offline solution. For instance, the SV can periodically flood the network with its location information or through the Automatic Identification System (AIS) [18]. On the basis of the SV location, a pre-computed offline route can be selected by each of the RBs. The proposed approach is viable since the SV moves at a very slow pace, and can even appear to be static from the perspective of a buoy that is several kilometers away.

[1]Given the deterministic and static nature of traffic in seismic surveying applications, it suffices to consider a D/D$^{[K_l]}$/1 model for analysis. However, in the case of adaptive data compression, for example, a more generalized G/D$^{[K_l]}$/1 batch service model must be considered for analysis.

3) CO-CHANNEL INTERFERENCE MITIGATION

With regards to the aspect of co-channel interference, the cell radius R may not be large enough to satisfy the condition in (3), so that the co-channel cells are located beyond the horizon. However, the impact of CCI can still be mitigated in such a scenario by exploiting the deterministic nature of traffic generated in seismic acquisition. As shown in Fig. 5, the data transmission periods in overlapping cells can be preemptively offset in the time domain. To ensure continued queue stability, the total sum of the data transmission periods must not exceed the minimum of the sleep periods across the co-channel cells. With reference to the l^{th} link, let $\mathcal{I}_l$ denote the set of co-channel cells. Then, the necessary condition can be expressed as

$$\sum_{l' \in \mathcal{I}_l}^{N} t_{l',d}(\boldsymbol{\phi}_{l'}) < \min \left\{ t_{l'',sl} \right\} \quad \forall \ l'' \in \mathcal{I}_l \tag{19}$$

4) AN OPTIMIZATION FRAMEWORK FOR POWER CONSERVATION AT THE RBs

Based on the foregoing discussion, the following mixed-integer optimization problem is formulated with the objective of minimizing the sum power consumption of the network. For a given cell radius R, the total number of RBs required to provide coverage across the survey area can be found as per the topology described in Section III-B. A common value for the transmit power Υ and the MCS index η can be applied to all the inter-RB links to create a tractable problem, since a uniform hexagonal topology is employed across the survey area. Corresponding to each of the source RBs (that acquire data from the SBs), the following objective function is defined in (20), where $\mathbb{P}$ is defined as a master set of candidate paths.

$$\underset{[\Upsilon, \ \eta, \ K_1 \ \cdots \ K_{|\mathcal{P}|}, \ u_1 \ \cdots \ u_{|\mathbb{P}|}]}{\text{minimize}} \quad \sum_{\mathcal{P} \in \mathbb{P}} \sum_{l \in \mathcal{P}} u_\mathcal{P} P_l \tag{20}$$

$$t_{l,sl}(\boldsymbol{\phi}_l) \ \geq \ t_{sl}^{min} \quad \forall \ l \tag{21}$$

$$\mathcal{L}_\mathcal{P} \ \leq \ \mathcal{L}_{max} \tag{22}$$

$$\Gamma(\eta) \sum_{l' \in \mathcal{I}_l} K_{l'} < \frac{K_{l''}}{\lambda_{l''}} - \delta \quad \forall \ l \text{ and } l'' \in \mathcal{I}_l \tag{23}$$

$$\Upsilon_{min} \ \leq \ \Upsilon \ \leq \ \Upsilon_{max} \tag{24}$$

$$\eta_{min} \ \leq \ \eta \ \leq \ \eta_{max} \tag{25}$$

$$1 \ \leq \ K_l \ \leq \ K_{max} \quad \forall \ l \tag{26}$$

$$\Upsilon, \ \eta, \ K \ \in \ \mathbb{Z} \quad \forall \ l \tag{27}$$

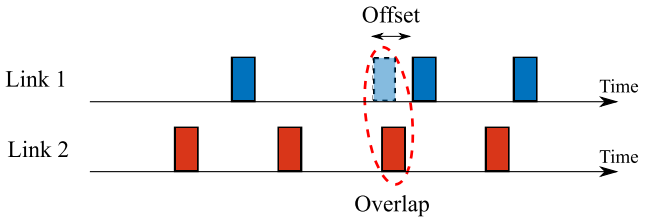

FIGURE 5. Circumventing an overlap in the data transmission periods through a preemptive time offset, in order to prevent co-channel interference.

$$u_{\mathcal{P}} \in \{0, 1\} \quad \forall\, \mathcal{P} \in \mathbb{P} \tag{28}$$

$$\sum_{\mathcal{P}\in\mathbb{P}} u_{\mathcal{P}} = 1 \tag{29}$$

Constraint (21) imposes a minimum sleep duration, and implicitly ensures a stable queue through (15). Real-time acquisition is mandated by constraint (22) through an upper-bound on the latency ($\mathcal{L}_{max}$), as perceived by the SV. Deriving from (19), constraint (23) ensures CCI-free operation. Lastly, the operating ranges for the decision variables are specified in (24)-(29). The binary decision variable $u_{\mathcal{P}}$ is introduced to model the choice of a single optimal path towards the SV.

The optimization problem in (20) is highly non-linear and non-convex. In order to yield a tractable problem, the inter-dependencies between the RBs can be eliminated by relaxing the latency constraint in (22) and setting $K_l = K_{max},\ \forall\, l$. A primary motivation for this relaxation is that the aggregation length is an adaptable parameter at the MAC layer, while it would be inconceivable to modify the number and topology of RBs on a frequent basis. Hence, the associated PHY-layer parameters such as R, η, and Υ can remain fixed for the duration of the survey, while the aggregation length can be adaptively tuned to meet the latency constraint at the SV.

As described in Algorithm 1, a linear optimization program can be rapidly solved to obtain optimal and offline values for the routing paths, R, η, and Υ. Note that an offline set of solutions are obtained for each position (or destination hop) that the SV assumes during the course of the survey. A latency constraint can then be reinstated to formulate the following convex minimization problem.

$$\underset{\left[K_1\ \cdots\ K_{|\hat{\mathcal{P}}|}\right]}{\text{minimize}} \quad \sum_{l\in\hat{\mathcal{P}}} P_l \tag{30}$$

$$t_{l,sl}(K_l, \hat{\eta}_l) \geq t_{sl}^{min} \quad \forall\, l \tag{31}$$

$$\sum_{l\in\hat{\mathcal{P}}} \left(\frac{K_l}{\lambda_l} - \delta\right) \leq \mathcal{L}_{max} \tag{32}$$

$$\Gamma(\hat{\eta}) \sum_{l'\in\mathcal{I}_l} K_{l'} \leq \frac{K_{l''}}{\lambda_{l''}} - \delta \quad \forall\, l \text{ and } l'' \in \mathcal{I}_l \tag{33}$$

where $\hat{\mathcal{P}}$ and $\hat{\eta}$ denote the optimal solution for the routing path and MCS index respectively, as given by Algorithm 1. Through the use of a numerical approximation technique in [15], the power consumption for a given link P_l was shown to be convex $\forall\ K_l \in [1, K_{max}]$. Hence, the objective function in (30) is convex. Based on the latency requirement ($\mathcal{L}_{max}$) at the SV, the optimal aggregation lengths can be found by solving (30) using standard convex optimization methods [35], [36].

Algorithm 1 Computation of Offline Parameters for the RBs

Define P_{total} to be the total power consumption (cost function)
Define a set $\mathbb{S}$ comprising all candidate positions of the SV
Initialize $K_l \leftarrow K_{max}\ \forall\, l$
for $s \in \mathbb{S}$ **do**
  Initialize $P_{min} \leftarrow \infty$
  for $\eta \in [\eta_{min}, \eta_{max}]$ **do**
    Initialize $\Upsilon \leftarrow \Upsilon_{max}$
    Solve for maximum value of R s.t. $p_{out}^{Ri} < p_{out,th}$
    while $p_{out}^{Ri} > p_{out,th}$ **do**
      $\Upsilon \leftarrow \Upsilon - \epsilon$
    end while
    $(P_{total}, \mathcal{P}) \leftarrow$ Solution of relaxed version of (20)
    if $P_{total} < P_{min}$ **then**
      $P_{min} \leftarrow P_{total}$
      $\hat{\mathcal{P}} \leftarrow \mathcal{P}$
      $\hat{R} \leftarrow R$
      $\hat{\eta} \leftarrow \eta$
      $\hat{\Upsilon} \leftarrow \Upsilon$
    end if
  end for
  Store offline solution set corresponding to the s^{th} position of the SV
end for

Overall, on the basis of the aforementioned cross-layer optimization framework, the proposed B-PSB scheme can minimize the total power consumption of the entire buoy-based backhaul network under a latency constraint. A key requirement for accurate operation of the B-PSB scheme is tight synchronization across all the RBs. This can be effectively achieved through the use of a navigation system that is nevertheless required for supporting the use of AUVs.

E. INTEGRATING AUTONOMOUS UNMANNED VEHICLES

Autonomous Unmanned Vehicles (AUVs) will serve as a vital component of marine OBS acquisition systems in the future. AUVs can be seamlessly integrated with *Wi-Buoy* and the B-PSB scheme. All RBs and the SV can be equipped with acoustic modems and navigation systems for facilitating AUV operation. Underwater acoustic communications for AUVs has been extensively analyzed in literature [37]. Given that data rates of only up to 30 Kbps can be achieved, real-time delivery of the recorded data cannot be sustained over such acoustic communication links. Hence, an AUV will have

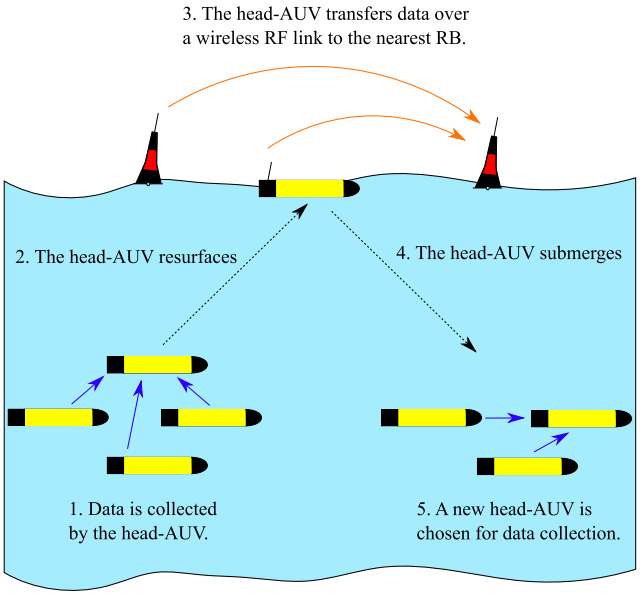

FIGURE 6. Resurfacing of the head-AUV.

to resurface and transfer all the recorded seismic data over a wireless (RF) link.

An illustration of such a resurfacing scheme is provided in Fig. 6. A round-robin approach can be employed to select a 'head-AUV' that first acquires data from the other AUVs via acoustic communication, and then resurfaces to transfer the amalgamated data to an RB (or the SV). During the ascent and descent of the head-AUV, the remaining AUVs can continue to record seismic data and prepare for the next resurfacing event. The head-AUV may also be chosen on the basis of the remaining amount of battery resources.

During its ascent, the head-AUV can be informed about the duty cycle and the channel being utilized by the RBs in a given cell. Accordingly, the head-AUV may decide to operate on an orthogonal duty cycle (in a TDMA-like manner) or operate as per the standards-prescribed CSMA/CA scheme when there is an overlap in the transmission duration. In Fig. 7a, a TDMA approach is favourable when the sleep duration of the RBs is much larger than the data transmission period. Alternatively, as shown in Fig. 7b, if the sleep period is of insufficient duration or a lower latency (for the AUV data) is demanded by the crew, the head-AUV may transmit using CSMA/CA.

IV. PERFORMANCE EVALUATION

The sweep length, listen time, and move-up time durations are taken to be 8 s, 6 s, and 10 s respectively, resulting in a total cycle time of 18 s. Given that the SV moves at a speed of around 5 knots ($\approx$ 10 kmph), a sweep would be conducted every 50 m which is in line with standard seismic acquisition methods [1]. The antenna height at the SV is taken to be 20 m, and 4-cell reuse is considered across the survey area.

The *ns-3* simulator is used for performance evaluation, and analytical solutions for the resource allocation problems

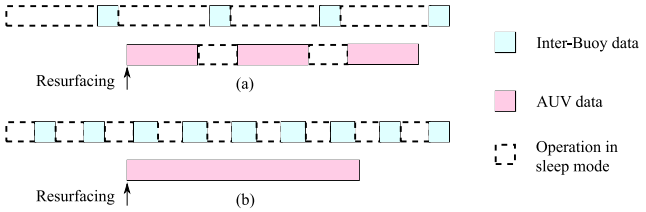

FIGURE 7. Two approaches to handling an AUV resurfacing event: (a) The AUV operates on an orthogonal duty cycle in a TDMA fashion. (b) When an overlap between transmissions is inevitable (due to a high arrival rate at the RBs), channel access can default to the EDCA scheme.

were obtained using MATLAB. A performance comparison is made between various versions of the IEEE 802.11 standard, each operating over a unique unlicensed range of frequencies. These include the 802.11af (television white space bands in 50-700 MHz), 802.11n (2.4 GHz bands), 802.11ax (5 GHz bands), and 802.11ad (60 GHz bands) standards, whose operating parameters have been listed under Table 2. The above standards have also been listed in increasing order of channel widths and PHY-layer data rates. As described in Section III-A, for the aforementioned frequency bands under consideration, large-scale fading effects are captured well by the two-ray model, and small-scale fading effects can be modelled by the Rician distribution [18]–[23]. In the case of IEEE 802.11ad, an additional atmospheric absorption loss of 17 dB/km is taken into account [15]. The IEEE 802.11ad standard is also reliant on the use of beamforming for optimizing the link budget, through periodic beam alignment via the use of phased arrays. The minimum required bit error rate is set to 10^{-7}, and the outage probability threshold $p_{out,th} = 10^{-5}$. Lastly, the power consumption parameters have been derived from [6], [38], [39].

A. SIMULATION RESULTS

The efficacy of the *Wi-Buoy* architecture is shown in Fig. 8, where a comparison is made between the power-optimized scenario (under the B-PSB scheme) and the classical scenario (no sleep duration is imposed on the buoys). Considering an antenna height of 1 m, under calm weather conditions, and $\mathcal{L}_{max} = 22$ s (data being acquired by the end of the subsequent sweep), it is seen that a reduction of nearly $81 - 92\%$ of the total power consumption can be achieved. Note that the presence (or absence) of a data point indicates whether real-time acquisition can (or cannot) be sustained at the given compression ratio. Additionally, the proposed analytical model is shown to be very effective, where the dashed curves (analysis) closely follow the trend of the solid curves (simulation).

A primary observation is that higher data rates lead to more effective power conservation under the B-PSB scheme. The 802.11ad standard can conserve the most amount of power, wherein the impact of Gigabit data transfer rates (implying a prolonged sleep duration) outweighs the shortcomings of a power-hungry chipset, and real-time acquisition

TABLE 2. List of simulation parameters.

Parameter	IEEE 802.11af [6]	IEEE 802.11n [6]	IEEE 802.11ax [38]	IEEE 802.11ad [39]
Operating Frequency	500 MHz	2.4 GHz	5.2 GHz	60 GHz
Bandwidth	8 MHz	20 MHz	80 MHz	2.16 GHz
Maximum EIRP	20 dBm	30 dBm		51 dBm
Antenna Gain	3 dB			46 dB
MCS Range	0–9	0–7	0–9	13–24
PHY-layer Data Rates	2.7–35.6 Mbps	7.2–72.2 Mbps	32.5–433.3 Mbps	0.7–6.7 Gbps
Current in Transmit Mode (at 0 dBm)	380 mA		562 mA	2776 mA
Current in Receive Mode	313 mA		418 mA	2198 mA
Current in Idle Mode	273 mA		399 mA	420 mA
Current in Sleep Mode	5 mA			
Supply Voltage	3 V			

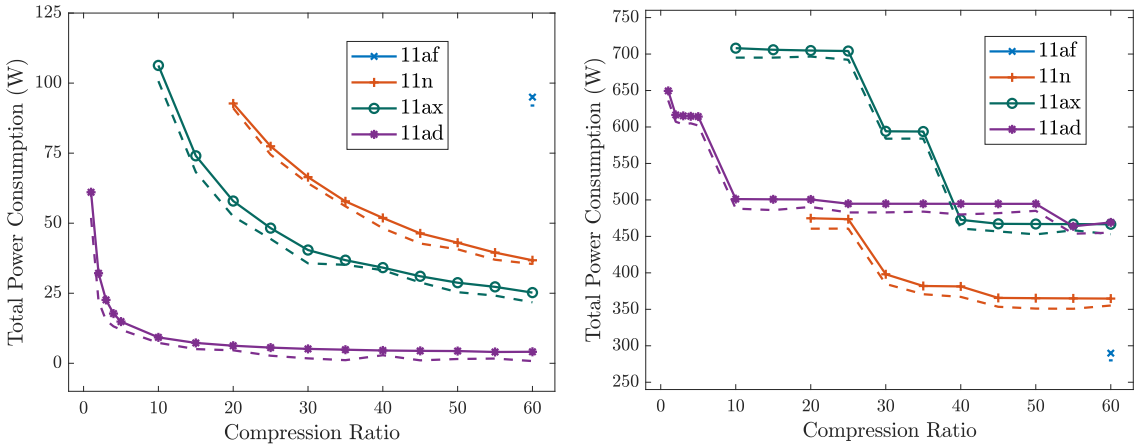

(a) Total power consumption in an optimized scenario (B-PSB scheme).

(b) Total power consumption in a classical scenario.

FIGURE 8. Performance gains achieved by the B-PSB scheme, along with a comparison between analysis and simulation.

can be achieved even with uncompressed data (compression ratio of 1). In stark contrast, the 802.11af standard operates at a much higher power consumption and can only sustain real-time acquisition at a compression ratio of 60. The 802.11n and 802.11ax standards attain intermediate performance, with a minimum required compression ratio of 20 and 10 respectively.

The total power consumption and average power consumption per RB are plotted in Fig. 9, for antenna heights of 1 m (Fig. 9a-9b) and 1.5 m (Fig. 9c-9d) as a function of the compression ratio. Each data point has been marked with the MCS index (Fig. 9a,9c) and the number of RBs (Fig. 9b,9d). With increasing values of the compression ratio, there is a decrease in the MCS index and the number of RBs, and consequently the total power consumption. This arises from the fact that the power savings obtained from a reduction of the number of RBs outweighs the marginal increase in power consumption introduced by the use of a lower MCS index. This also provides an explanation for an abrupt increase in the average power consumption per RB, which occurs when the compression ratio transitions from 25 to 30 (11n) and from 35 to 40 (11ax) in Fig. 9b, and from 20 to 25 (11n) in Fig. 9d. Furthermore, with reference to Fig. 9a and 9c, the use of a taller antenna height of 1.5 m can reduce the total power consumption as a result of operating at a higher MCS index and by reducing the total number of RBs. However, taller antenna heights present logistical challenges in terms of the buoy dimensions and weight.

When small values for the compression ratio ($\leq$ 10) are desired by the crew, the use of higher data rates via the IEEE 802.11ad standard is imperative to effective power conservation and real-time acquisition. However, if the data quality requirements are not as stringent (compression ratio $\geq$ 30), an increase in the data rate provides diminishing returns on the average power consumption, which is the sole parameter that determines the operating time of the RBs (until recharging is required). In such a scenario, it may be feasible to employ the use of the 802.11n or 802.11ax standards as well, albeit with a higher number of RBs.

The impact of a stricter latency constraint, wind speed, and antenna height, on the total power consumption is illustrated in Fig. 10. The value of $\mathcal{L}_{max}$ is set to 4 s to impose a stricter latency constraint such that the data is acquired by the end of the current sweep. A comparison between Fig. 8a and Fig. 10a

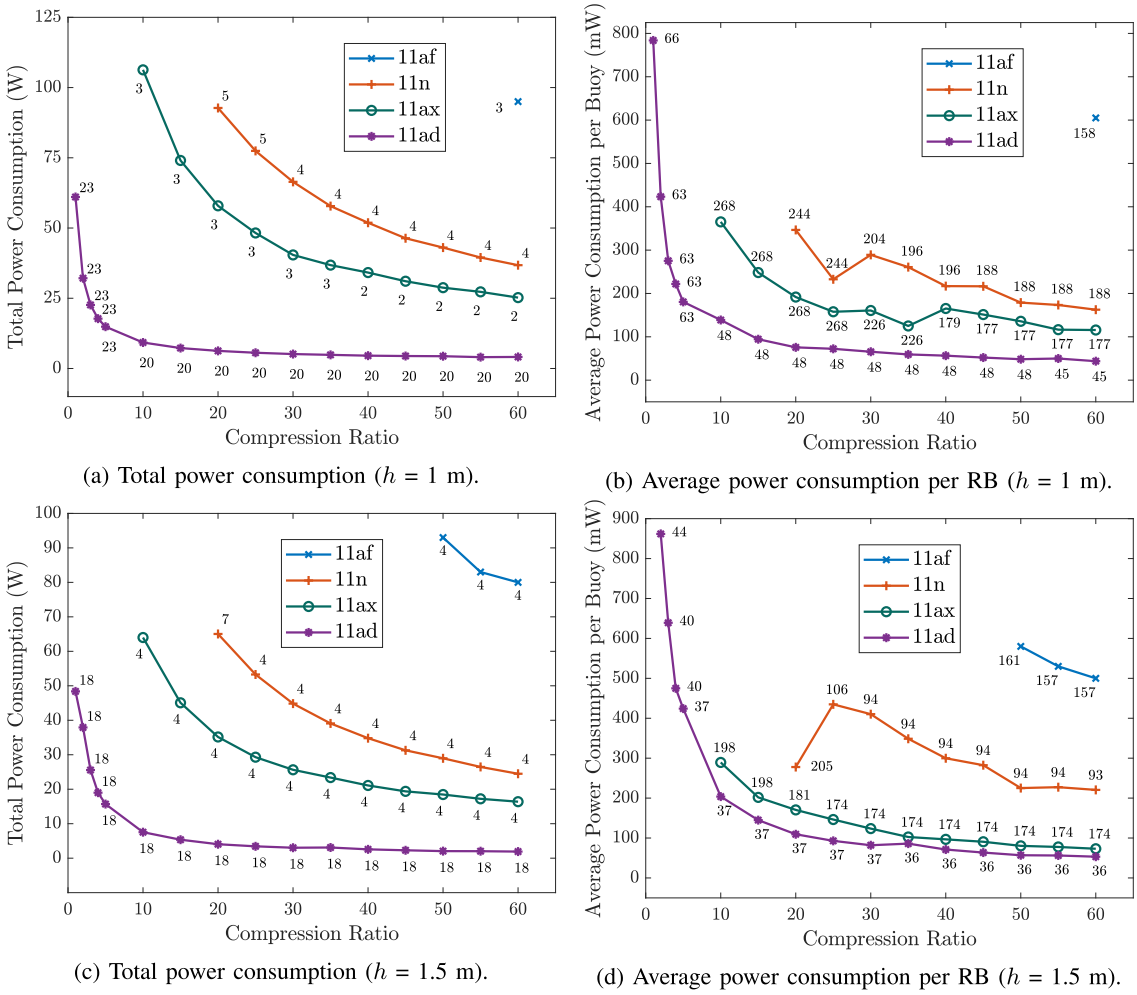

(a) Total power consumption (h = 1 m).

(b) Average power consumption per RB (h = 1 m).

(c) Total power consumption (h = 1.5 m).

(d) Average power consumption per RB (h = 1.5 m).

FIGURE 9. **Power consumption performance of the proposed *Wi-Buoy* architecture.**

shows that more power is consumed as a result of a lower latency requirement, since the duration of sleep is reduced. It can also be seen that the IEEE 802.11af standard cannot meet the lower latency requirement, even at a compression ratio of 60.

As described in [16], three Sea State Codes (SSCs) are considered – *Smooth* (wind speed of 9 kmph), *Slight* (wind speed of 16 kmph), and *Moderate* (wind speed of 35 kmph). For an antenna height of 1 m, the variation in the total power consumption, as a function of the SSCs, can be seen through Fig. 10a-10c. Overall, an increase in the wind speed leads to a larger value for p_{out}, resulting in a higher acquisition time in (8). This in turn reduces the maximum achievable sleep duration in (16) and the resultant power conservation performance. In particular, the latency requirement cannot be met at compression ratios of 10 (802.11ax) and 20 (802.11n) in the case of slight and moderate SSCs. For an antenna height of 1.5 m, the overall power consumption remains relatively unaffected (a marginal increase of $1-2\%$), implying that the impact of wind speed can be effectively tackled via the use of taller antenna heights.

A performance analysis is presented in Fig. 11 for an AUV-resurfacing event based on the use of IEEE 802.11ax with an antenna height of 1.5 m. A group of 25 AUVs is considered with each AUV towing a streamer of eight 4C sensors. The head AUV is polled to resurface every 30 minutes, which is equivalent to the cycle length of around 100 sweeps. The average power consumption is shown for three scenarios, where the upper plot represents a cell adjacent to the SBs (low arrival rate), the middle plot represents a cell in the central region of survey area (moderate arrival rate), and the bottom plot represents the final cell comprising the SV (very high arrival rate). Naturally, the power consumption increases from top to bottom, due to an increase in the arrival rate which in turn yields a shorter sleep duration at the RBs. For the most part, the TDMA-based approach works well and the head-AUV can resurface without introducing additional interference and preventing any increase in the power consumption of the RBs. After resurfacing, the latency in receiving the AUV data is also minimal, with a value lesser than 0.4 s. However, for a compression ratio in the range of 10–25, CSMA/CA has to be applied in the high-rate cell, which leads

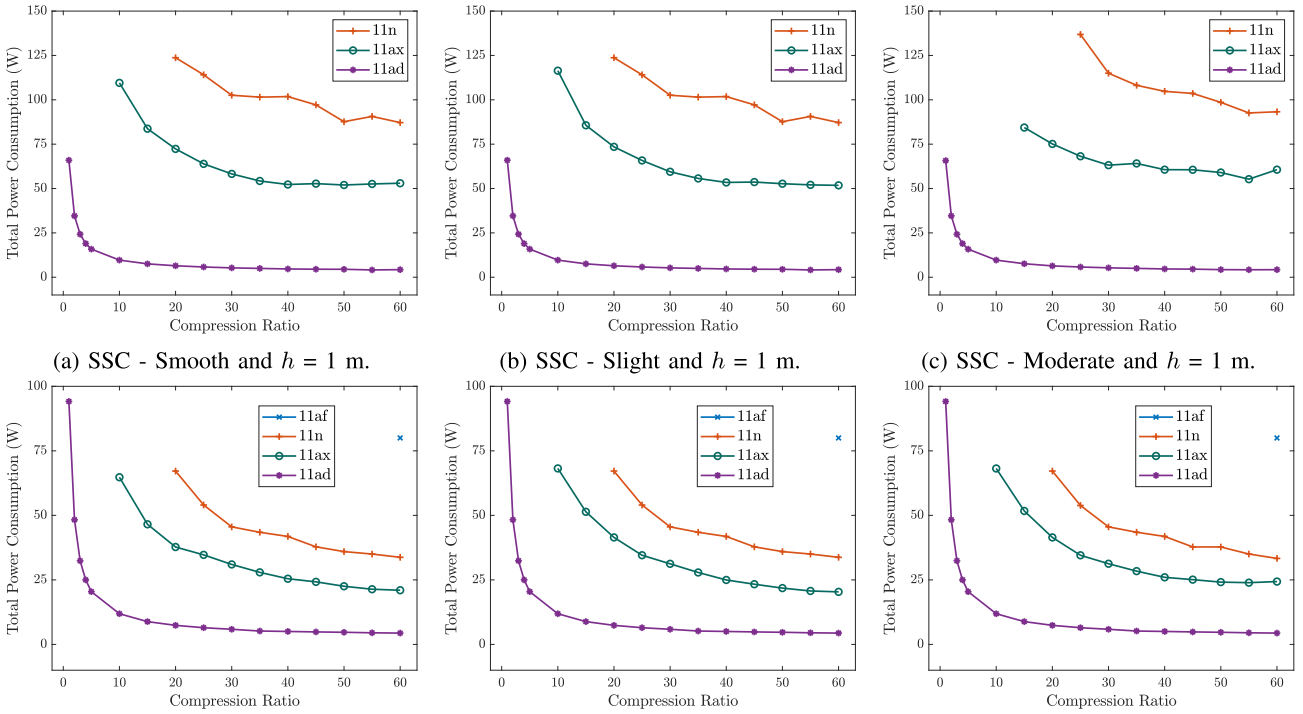

(a) SSC - Smooth and h = 1 m. (b) SSC - Slight and h = 1 m. (c) SSC - Moderate and h = 1 m.

(d) SSC - Smooth and h = 1.5 m. (e) SSC - Slight and h = 1.5 m. (f) SSC - Moderate and h = 1.5 m.

FIGURE 10. Power consumption performance as a function of the wind speed and the antenna height.

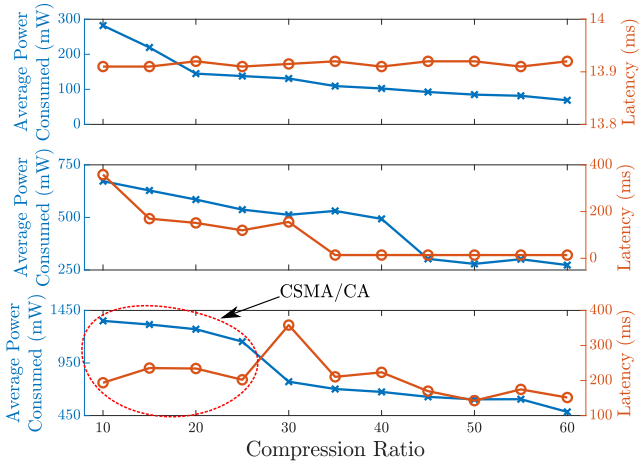

FIGURE 11. Data collection from an AUV in conjunction with the B-PSB scheme.

to a sudden increase in the power consumed. Although such a resurfacing event would occur only once every 100 sweeps and the overhead in terms of the power consumption may be deemed negligible, it would be preferable for the head-AUV to resurface in a cell having a low arrival rate of packets at the RBs.

V. CONCLUSION

A comprehensive overview is offered on marine seismic acquisition and the requirements imposed by a wireless buoy-based network architecture. Despite a data generation rate of several Gigabits per second, the proposed *Wi-buoy* architecture can sustain real-time data delivery in an energy-efficient, scalable, and standards-compliant manner. A cross-layer optimization approach is incorporated into the B-PSB scheme, that minimizes the total power consumption and enhances the operational life of the survey. A performance comparison between various versions of the IEEE 802.11 standard reveals that high-rate protocols such as 802.11ad are necessary for the delivery of uncompressed seismic data, while the 802.11n and 802.11ax standards exhibit reasonable performance when a compression ratio of 30 or greater can be tolerated. The impact of wind speed and antenna height on the performance of *Wi-Buoy* has been studied as well. AUVs can be integrated into the *Wi-buoy* architecture where it is seen that low latency operation can be conducted in cells having a low arrival rate of packets. Overall, this article provides the foundational framework for upcoming wireless marine seismic systems and other related data-intensive applications in the maritime environment.

APPENDIX

The second and third terms of the expression for P_l in (18) can be written in the form

$$f(\lambda_l) = \frac{\alpha\lambda_l}{K_l - \lambda_l\delta} \tag{34}$$

where $\alpha > 0$, since $\gamma_d \gg \gamma_{idle} > \gamma_{sl}$. Taking the first derivative of $f(\lambda_l)$ with respect to λ_l,

$$\frac{\partial f(\lambda_l)}{\partial \lambda_l} = \frac{\alpha K_l}{(K_l - \lambda_l\delta)^2} > 0 \tag{35}$$

Since $\frac{\partial f(\lambda_l)}{\partial \lambda_l} > 0$, $\forall \lambda_l > 0$, it can be inferred that P_l monotonically increases with λ_l.

REFERENCES

[1] D. Dondurur, *Acquisition and Processing of Marine Seismic Data*. Amsterdam, The Netherlands: Elsevier, 2019.

[2] W. Yi, S. Grion, and R. Bale, "What comes up must have gone down: The principle and application of up-down deconvolution for multiple attenuation of ocean bottom data," *CSEG Recorder*, vol. 34, no. 10, pp. 10–16, Dec. 2009.

[3] K. Karlsen, "System and method for wireless data collection from seismic recording buoys," U.S. Patent 7 466 627, Dec. 16, 2008.

[4] ION Geophysical Corporation. (Accessed: Sep. 15, 2021). *VSO II*. Accessed: 2011. [Online]. Available: https://www.iongeo.com/virtuals/ResourceArchives/content/documents/Resource%20Center/Brochures%20and%20Data%20Sheets/Data%20Sheets/Marine%20Systems/Product%20Sheets/PS_MIS_VSOII.pdf

[5] G. Cambois, S. A. Mesaabi, G. A. Casson, J. Cowell, M. Mahgoub, and A. A. Kobaisi, "The world's largest continuous 3D onshore and offshore seismic survey sets ambitious quality and turnaround targets," in *Proc. SEG Tech. Program Expanded Abstr.*, 2019, pp. 12–16.

[6] V. A. Reddy, G. L. Stuber, S. Al-Dharrab, W. Mesbah, and A. H. Muqaibel, "A wireless geophone network architecture using IEEE 802.11af with power saving schemes," *IEEE Trans. Wireless Commun.*, vol. 18, no. 12, pp. 5967–5982, Dec. 2019.

[7] D. B. Crice, "Systems and methods for seismic data acquisition," U.S. Patent 9 291 732, Mar. 22, 2016.

[8] S. Savazzi, U. Spagnolini, L. Goratti, D. Molteni, M. Latva-Aho, and M. Nicoli, "Ultra-wide band sensor networks in oil and gas explorations," *IEEE Commun. Mag.*, vol. 51, no. 4, pp. 150–160, Apr. 2013.

[9] K.-L.-A. Yau, A. R. Syed, W. Hashim, J. Qadir, C. Wu, and N. Hassan, "Maritime networking: Bringing internet to the sea," *IEEE Access*, vol. 7, pp. 48236–48255, 2019.

[10] S. Jiang, "Marine internet for internetworking in oceans: A tutorial," *Future Internet*, vol. 11, no. 7, p. 146, Jul. 2019.

[11] M. F. D. de Guzman, C. A. G. Hilario, R. V. P. Vistal, I. C. Mosquera, J. M. Judan, and J. J. S. Marciano, "Alternative backhaul link for community cellular network in rural coastal areas," in *Proc. IEEE Global Humanitarian Technol. Conf. (GHTC)*, Oct. 2019, pp. 1–6.

[12] A. Hosseini-Fahraji, P. Loghmannia, K. Zeng, X. Li, S. Yu, S. Sun, D. Wang, Y. Yang, M. Manteghi, and L. Zuo, "Energy harvesting long-range marine communication," in *Proc. IEEE Conf. Comput. Commun. (IEEE INFOCOM)*, Jul. 2020, pp. 2036–2045.

[13] Y. Wang, W. Feng, J. Wanga, and T. Q. S. Quek, "Hybrid satellite-UAV-terrestrial networks for 6G ubiquitous coverage: A maritime communications perspective," *IEEE J. Sel. Areas Commun.*, early access, Jun. 14, 2021, doi: 10.1109/JSAC.2021.3088692.

[14] C. Tsingas, T. Brizard, and A. A. Muhaidib, "Seafloor seismic acquisition using autonomous underwater vehicles," *Geophys. Prospecting*, vol. 67, no. 6, pp. 1557–1570, Jul. 2019.

[15] V. A. Reddy, G. L. Stüber, S. Al-Dharrab, W. Mesbah, and A. H. Muqaibel, "Energy-efficient mm-wave backhauling via frame aggregation in wide area networks," *IEEE Trans. Wireless Commun.*, early access, May 17, 2021, doi: 10.1109/TWC.2021.3079345.

[16] *Guide to Meteorological Instruments and Methods of Observation*. World Meteorol. Org., Geneva, Switzerland, 2018.

[17] A. Payani, A. Abdi, X. Tian, F. Fekri, and M. Mohandes, "Advances in seismic data compression via learning from data: Compression for seismic data acquisition," *IEEE Signal Process. Mag.*, vol. 35, no. 2, pp. 51–61, Mar. 2018.

[18] J. Wang, H. Zhou, Y. Li, Q. Sun, Y. Wu, S. Jin, T. Q. S. Quek, and C. Xu, "Wireless channel models for maritime communications," *IEEE Access*, vol. 6, pp. 68070–68088, 2018.

[19] W. Xu, H. Zhou, T. Yang, H. Wu, and S. Guo, "Proactive link adaptation for marine Internet of Things in TV white space," in *Proc. IEEE Int. Conf. Commun. (ICC)*, Jun. 2020, pp. 1–6.

[20] J.-H. Lee, J. Choi, W.-H. Lee, J.-W. Choi, and S.-C. Kim, "Measurement and analysis on land-to-ship offshore wireless channel in 2.4 GHz," *IEEE Wireless Commun. Lett.*, vol. 6, no. 2, pp. 222–225, Apr. 2017.

[21] W. Wang, R. Raulefs, and T. Jost, "Fading characteristics of ship-to-land propagation channel at 5.2 GHz," in *Proc. OCEANS Shanghai*, Apr. 2016, pp. 1–7.

[22] N. Mehrnia and M. K. Ozdemir, "Novel maritime channel models for millimeter radiowaves," in *Proc. 24th Int. Conf. Softw., Telecommun. Comput. Netw. (SoftCOM)*, Sep. 2016, pp. 1–6.

[23] X. Cao and T. Jiang, "Research on sea surface Ka-band stochastic multipath channel modeling," in *Proc. 3rd Asia–Pacific Conf. Antennas Propag.*, Jul. 2014, pp. 675–678.

[24] G. L. Stüber, *Principles of Mobile Communication*, 4th ed. New York, NY, USA: Springer, 2017.

[25] A. Shahanaghi, Y. Yang, and R. M. Buehrer, "Stochastic link modeling of static wireless sensor networks over the ocean surface," *IEEE Trans. Wireless Commun.*, vol. 19, no. 6, pp. 4154–4169, Jun. 2020.

[26] E. Dinc and O. B. Akan, "Beyond-line-of-sight communications with ducting layer," *IEEE Commun. Mag.*, vol. 52, no. 10, pp. 37–43, Oct. 2014.

[27] *IEEE Standard for Information Technology—Part 11: Wireless LAN Medium Access Control (MAC) and Physical Layer (PHY) Specifications*, IEEE Standard 802.11-2020, Feb. 2021, pp. 1–4379.

[28] A. Rao and I. Stoica, "An overlay MAC layer for 802.11 networks," in *Proc. 3rd Int. Conf. Mobile Syst., Appl., Services (MobiSys)*. New York, NY, USA: ACM, 2005, pp. 135–148.

[29] P. Djukic and P. Mohapatra, "Soft-TDMAC: A software TDMA-based MAC over commodity 802.11 hardware," in *Proc. 28th Conf. Comput. Commun. (IEEE INFOCOM)*, Apr. 2009, pp. 1836–1844.

[30] J. Snow, W.-C. Feng, and W.-C. Feng, "Implementing a low power TDMA protocol over 802.11," in *Proc. IEEE Wireless Commun. Netw. Conf.*, vol. 1, Mar. 2005, pp. 75–80.

[31] A. S. Ivanov, A. I. Lyakhov, and E. M. Khorov, "A mathematical model of transmitting a non-ordinary flow with periodic reservations and block acknowledgements in a channel with correlated noise," *Autom. Remote Control*, vol. 78, no. 11, pp. 1978–1990, Nov. 2017.

[32] E. Khorov, A. Lyakhov, A. Ivanov, and I. F. Akyildiz, "Modeling of real-time multimedia streaming in Wi-Fi networks with periodic reservations," *IEEE Access*, vol. 8, pp. 55633–55653, 2020.

[33] S. Ross, *Introduction to Probability Models*, 7th ed. New York, NY, USA: Academic, 2014.

[34] R. Palacios, F. Granelli, D. Kliazovich, L. Alonso, and J. Alonso-Zarate, "An energy efficient distributed coordination function using bidirectional transmissions and sleep periods for IEEE 802.11 WLANs," in *Proc. IEEE Global Commun. Conf. (GLOBECOM)*, Dec. 2013, pp. 1619–1625.

[35] S. Boyd and L. Vandenberghe, *Convex Optimization*. Cambridge, U.K.: Cambridge Univ. Press, 2004.

[36] J. Kronqvist, D. E. Bernal, A. Lundell, and I. E. Grossmann, "A review and comparison of solvers for convex MINLP," *Optim. Eng.*, vol. 20, no. 2, pp. 397–455, Jun. 2019.

[37] M. Y. I. Zia, J. Poncela, and P. Otero, "State-of-the-art underwater acoustic communication modems: Classifications, analyses and design challenges," *Wireless Pers. Commun.*, vol. 116, no. 2, pp. 1325–1360, Jan. 2021.

[38] V. A. Reddy, G. L. Stüber, S. Al-Dharrab, A. H. Muqaibel, and W. Mesbah, "Wireless backhaul strategies for real-time high-density seismic acquisition," in *Proc. IEEE Wireless Commun. Netw. Conf. (WCNC)*, May 2020, pp. 1–7.

[39] T. Sowlatiet, S. Sarkar, B. G. Perumana, W. L. Chan, A. P. Toda, B. Afshar, M. Boers, D. Shin, T. R. Mercer, W. H. Chen, and A. G. Besoli, "A 60-GHz 144-element phased-array transceiver for backhaul application," *IEEE J. Solid-State Circuits*, vol. 53, no. 12, pp. 3640–3659, Dec. 2018.

VARUN AMAR REDDY received the B.Tech. degree in electronics and communication engineering from the National Institute of Technology Karnataka, Surathkal, India, in 2016, and the Ph.D. degree in electrical and computer engineering from Georgia Institute of Technology, Atlanta, USA, in 2021. He is currently a Senior Systems Engineer with Qualcomm Wireless Research Group, San Diego, USA. His research interests include wireless networking, access protocol design, energy-efficient communications, and next-generation positioning systems. He has been granted one U.S. patent. He has served as a Reviewer for IEEE TRANSACTIONS ON VEHICULAR TECHNOLOGY, IEEE ACCESS, and various IEEE conferences.

GORDON L. STÜBER (Fellow, IEEE) received the B.A.Sc. and Ph.D. degrees in electrical engineering from the University of Waterloo, Waterloo, ON, Canada, in 1982 and 1986, respectively.

In 1986, he joined the School of Electrical and Computer Engineering, Georgia Institute of Technology, where he is currently the Joseph M. Pettit Chair Professor of communications. He is the author of the wireless textbook: *Principles of Mobile Communication* (Kluwer Academic Publishers, 1996, 2nd ed. 2001, 3rd ed. 2011, 4th ed. 2017).

Dr. Stüber became an IEEE Fellow, in 1999, for contributions to mobile radio and spread spectrum communications. He was a past member of the IEEE Communications Society Awards Committee, from 1999 to 2002. He was an Elected Member-at-Large on the IEEE Communications Society Board of Governors, from 2007 to 2009, and is an Elected Member of the IEEE Vehicular Technology Society Board of Governors, from 2001 to 2021. He was a corecipient of the Jack Neubauer Memorial Award, in 1997, for the best systems paper published in the IEEE TRANSACTIONS ON VEHICULAR TECHNOLOGY, and the Neal Shepherd Memorial Best Propagation Paper Award, in 2012, for the best propagation paper published in the IEEE TRANSACTIONS ON VEHICULAR TECHNOLOGY. He was a recipient of the IEEE Vehicular Technology Society's James R. Evans Avant Garde Award, in 2003, for contributions to theoretical research in wireless communications, the 2007 IEEE Communications Society Wireless Communications Technical Committee Recognition Award for outstanding technical contributions in the field and for service to the scientific and engineering communities, the 2017 IEEE ComSoc RCC Technical Recognition Award for outstanding research contributions to radio communications, and the IEEE Vehicular Technology Society Outstanding Service Award, in 2005. He was an IEEE Communication Society Distinguished Lecturer, from 2007 to 2008, and an IEEE Vehicular Technology Society Distinguished Lecturer, from 2010 to 2012. He was the Technical Program Chair of the 1996 IEEE Vehicular Technology Conference (VTC'96) and the 1998 IEEE International Conference on Communications (ICC'98), the General Chair of the Fifth IEEE Workshop on Multimedia, Multiaccess and Teletraffic for Wireless Communications (MMT'00), the 2002 IEEE Communication Theory Workshop (CTW'02), and the Fifth YRP International Symposium on Wireless Personal Multimedia Communications (WPMC'02), and the General Co-Chair of the 2019 IEEE 90th Vehicular Technology Conference (VTC2019-Fall). He is a past Editor for Spread Spectrum of the IEEE TRANSACTIONS ON COMMUNICATIONS, from 1993 to 1998.